Materials Horizons

Low Voltage Induced Reversible Magnetoelectric Coupling in Fe3O4 Thin Films for Voltage Tunable Spintronic Devices

Journal:	*Materials Horizons*
Manuscript ID	MH-COM-06-2018-000763.R2
Article Type:	Communication
Date Submitted by the Author:	05-Aug-2018

Complete List of Authors:	Zhang, Le; Xi'an Jiaotong University, Hou, Weixiao; Xi'an Jiaotong University Dong, Guohua; Xi'an jiaotong University Zhou, Ziyao; Xi'an Jiaotong University Zhao, Shishun; Xi'an Jiaotong University , School of Electronic and Information Engineering Hu, Zhongqiang; Xi'an Jiaotong University, Ren, Wei; Xi'an Jiaotong University, Chen, Mingfeng; Tsinghua University Nan, Cewen; Tsinghua University Ma, Jing; Tsinghua University, School of Materials Science and Engineering Zhou, Hua; Argonne National Lab, Advanced Photon Source Chen, Wei; Argonne National Laboratory, Institute for Molecular Engineering and Materials Science Division; University of Chicago, Institute for Molecular Engineering Ye, Z.-G; Simon Fraser University, Department of Chemistry Jiang, Zhuangde; Xi'An Jiaotong University, School of Mechanical Engineering Liu, Ming; Xi'an Jiaotong University,

SCHOLARONE™
Manuscripts

Low Voltage Induced Reversible Magnetoelectric Coupling in Fe_3O_4 Thin Films for Voltage Tunable Spintronic Devices

Le Zhang[1], Weixiao Hou[1], Guohua Dong[1], Ziyao Zhou[1*], Shishun Zhao[1], Zhongqiang Hu[1], Wei Ren[1*], Mingfeng Chen[2], Ce-Wen Nan[2], Jing Ma[2], Hua Zhou[3], Wei Chen[4, 5], Zuo-Guang Ye[6, 1], Zhuang-De Jiang[7], Ming Liu[1*]

1. Electronic Materials Research Laboratory, Key Laboratory of the Ministry of Education, School of Electronic and Information Engineering, State Key Laboratory for Mechanical Behavior of Materials, Xi'an Jiaotong University, Xi'an 710049, China
2. Department of Materials Science and Engineering, State Key Lab of New Ceramics and Fine Processing, Tsinghua University, Beijing 100084, China
3. Advanced Photon Source, Argonne National Laboratory, Lemont, Illinois 60439, United States
4. Institute for Molecular Engineering and Materials Science Division, Argonne National Laboratory, Lemont, Illinois 60439, United States
5. Institute for Molecular Engineering, the University of Chicago, Chicago, Illinois 60637, United States
6. Department of Chemistry and 4D LABS, Simon Fraser University, Burnaby, British Columbia V5A 1S6, Canada
7. State Key Laboratory for Manufacturing Systems Engineering, Xi'an Jiaotong University, Xi'an 710049, Shaanxi, China

Abstract

The ongoing demands for efficient and low-energy consumption spintronic devices motivate the idea of manipulating magnetism by ionic liquid (IL) electrolyte gating at

low voltage. Although magnetoelectric (ME) coupling has already been realized in some field-effect-transistor (FET) structures, some vital parameters such as giant ME coupling coefficient, excellent reversibility and low gating voltage seldom come at the same time, which greatly suppress the industrialization. Here we demonstrate a large 552 Oe spin dynamics modulation of Fe_3O_4 thin film induced at gating voltage V_g= +1.5 V in an IL-gated Au/[DEME]$^+$[TFSI]$^-$/Fe_3O_4/MgO heterostructure with good reversibility up to 80 cycles, giving rise to a high ME coefficient of 368 Oe/V. Such large ME tunability under low V_g could be attributed to the electric field (E-field) induced ionic transformation between Fe^{2+} and Fe^{3+} at the interface. The tiny thickness change (~2 angstrom) and roughness change of Fe_3O_4 films under V_g= +1.5 V illustrated by *in*-situ X-ray Reflection (XRR) give a reasonable explanation on the outstanding reversible property. Interestingly, it is found that the Verwey transition temperature of Fe_3O_4 has a strong dependence on V_g, revealing the potential of IL gating control of the intrinsic spin ordering inside magnetic films. This work drives forward the low-voltage induced reversible ME coupling to high-performance spintronic devices.

Keywords: Magnetoelectric coupling, Voltage control of magnetism, Ferromagnetic resonance, Ionic liquid gating

Introduction

High-performance spintronic devices with low energy consumption, adequate reversibility and fast response are greatly demanded for the evolving technology because spintronics offer opportunities for a new generation of devices combining standard microelectronics with spin-dependent effects that arise from the interaction between spin of the carrier and the magnetic properties of the material[1-10]. Voltage-induced magnetoelectric (ME) coupling in field-effect transistors (FET) at the interface opens up a new way to comprehend the fundamental science and design advanced spintronic devices. However, voltage-tunable ME devices on integrated circuit (IC) requires digital operation voltage (<5 V), which is too low to drive the bulk piezoelectric-based multiferroics[11-16].

As one of the cutting-edge voltage tuning technologies, ionic liquid (IL) electrolyte gating has made great developments in manipulating p-n junction, band insulator, insulator-to-metal transition, carrier delocalization and transport properties of the semiconductor through vigorous ion transmission in an ideal Field Effect Transistor (FET) structure[3, 17-19]. In particular, IL gating is also very effective in the modifications of magnetic properties such as magnetoresistance, magnetization and magnetic anisotropy, and in spin wave and spin dynamics[3,20-24], where the spin behavior is sensitive to interfacial charge doping. During the IL gating process, modification of spin, charge, orbital, lattice and interactions among them induced by electric double layer (EDL) at atomic or subatomic level enables exotic phenomena and novel spintronics/electronics devices with additional degrees of freedom[18,25-27].

Interfacial ME coupling effect offers an effective approach for controlling the surface magnetism in various oxide gating structures with large ME tunability at low applied voltage[3,26,28-32]. Recently, Yu et al.[33] reported an E-field induced tri-phase transformation in $SrCoO_{2.5}$ via ionic doping (O^{-2}, H^{+}) through IL gating, enabling a smart tuning of electronic, optical or magnetic properties with great application potential in various fields. Clearly, this achievement proves that the IL gating of magnetic oxides systems are worth further studying because the magnetism of oxides are highly depended on chemical valences, which can easily be manipulated by ions transmitting during the IL gating process. Furthermore, precise determination of voltage control of magnetic anisotropy (VCMA) with excellent reversible performances still remains challenging for functional devices.

Magnetite (Fe_3O_4) is a well-studied magnetic oxide with cubic inverse spinel structure, and has a conducting spin-polarized ferrimagnet with enriched physics and chemistry phenomena. The coexistence of Fe^{2+} and Fe^{3+} mixed valences creates various phases (FeO, α-Fe_2O_3, γ-Fe_2O_3), and corresponding plentiful magnetic, electrical and optical properties[34,35]. Magnetite thin films also attract great attentions for their broadly application potential on electronics, spintronics and biology[36-39]. Moreover Fe_3O_4 are more suitable for the spintronics application due to the lower cost, the higher abundance of iron and the lattice constant matching widely used substrates like MgO(001) and other oxide compounds. Tuning the magnetism of Fe_3O_4 electrically in a fast, compact and energy efficient manner is thereby critical to realize next generation Fe_3O_4 based spintronic devices. In this work, we realized a

precisely-determined 552 Oe spin dynamics modulation (ferromagnetic resonance field shift, FMR H_r) via a small Vg (+1.5 V) with good reversibility in an IL/Fe_3O_4/MgO heterostructure, corresponding to a large ME tunability of 368 Oe/V, which is 2 orders of magnitude greater than that of strain-mediated ME structures in previous reported 2.15 Oe/V in Fe_3O_4/PZN-PT heterostructure[11]. The attained ME coupling coefficient is also higher than the recently reported record values in our previous research[3] on Co and the mostly reported 226 Oe/V on $La_{0.74}Sr_{0.26}MnO_3$ gated with IL[2]. This IL gating of magnetite process shows a great reversibility after 80 cycles test. Both chemical and structural analyses indicate that the modulation of magnetism–spin dynamics is originated from E-field induced interfacial ionic chemical valence switching (between Fe^{2+} and Fe^{3+}). The tiny thickness change (~2 angstrom) and roughness change of Fe_3O_4 films after gated at V_g= +1.5 V illustrated by *in*-situ XRR give a reasonable explanation on the outstanding reversible property. In addition, the Verwey transition temperature of Fe_3O_4 can be also shifted by 6 K with IL gating, which is worthy further investigation for its capability of manipulating the intrinsic spin ordering. IL gating control of magnetite is therefore proven to be a great E-field modulation technology that allows essential modulation of magnetism and enables voltage-tunable spintronics/electronics applications with advanced functionality.

Results and discussion

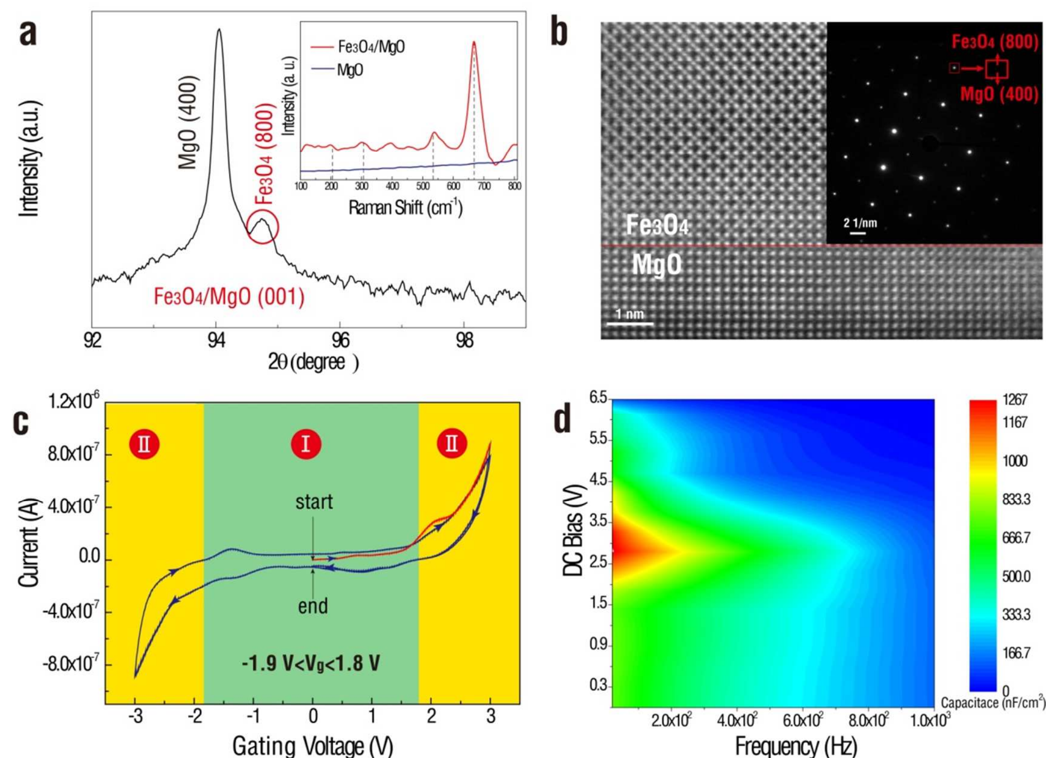

Figure 1. (a) X-ray diffraction patterns of the Fe_3O_4/MgO heterostructure. The inset shows the Raman spectra of the heterostructure. (b) Representative HRTEM images at the Fe_3O_4/MgO interface. The inset shows the selected area electron diffraction profile and the red square shows the overlapped electron diffraction spots of Fe_3O_4 (800) films and MgO (400) substrate. (c) $[DEME]^+[TFSI]^-$ electrochemical window test. The V_g ranges were divided into Region I (-1.9 V < V_g < 1.8 V) and Region II ($V_g \geq$ 1.8 V or $V_g \leq$ -1.9 V). (d) Frequency dependence of the capacitance of $[DEME]^+[TFSI]^-$ from 20 Hz to 1000 Hz at different DC bias from 0 V to 6.5 V with the same AC voltage of 100 mV.

The XRD θ-2θ scan for the (001)-oriented Fe_3O_4/MgO heterostructure demonstrates that the magnetic films are fully textured along the [001] orientation without other phases or textures, as shown in Figure 1a with the intensity in log scale.

A broader XRD pattern is also shown in Supporting Information in Figure S1a. The inset in Figure 1a displays the Raman spectra of the heterostructure, where the dash lines indicate the characteristic peaks of magnetite, confirming the formation of the Fe_3O_4 phase. Combining the XRD and Raman spectra, we can conclude that the magnetite films were successfully epitaxially deposited on the MgO substrates. The microstructure of the Fe_3O_4/MgO heterostructure was imaged by spherical aberration-corrected electron microscopy (SAEM). The different scale cross-sectional high-resolution transmission electron microscopy (HRTEM) images in Figure S1b-e (Supporting Information) show sharp interface between the Fe_3O_4 films and the MgO substrate. The perfect epitaxial growth is illustrated by the enlarged HRTEM image at the Fe_3O_4/MgO interface, as shown in Figure 1b. The inset in Figure 1b displays the selected area electron diffraction, in which the red square shows overlapped diffraction spots composed of Fe_3O_4 (800) films and MgO (400) substrate. Figure 1c displays the IL gating electrochemical window test, in which the applied V_g is divided into two regions: Region I (-1.9 V$<V_g<$1.8 V, $|I| < 2 \times 10^{-7}$ A, within electrochemical window) and Region II ($V_g \geq$1.8 V or $V_g \leq$ -1.9 V, $|I| \geq 2 \times 10^{-7}$ A, outside the electrochemical window). To characterize the dielectric properties of the IL, the frequency-dependent capacitance of $[DEME]^+[TFSI]^-$ is measured from 20 Hz to 1000 Hz at different direct current (DC) bias (from 0 V to 6.5 V) with the same alternating current (AC) level (100 mV), as shown in Figure 1d. It is easy to find out that the greatest capacitance of ~1275 nF/cm^2 is achieved when the DC bias is around 3.0 V, corresponding to the highest interface charges accumulation during the gating

process.

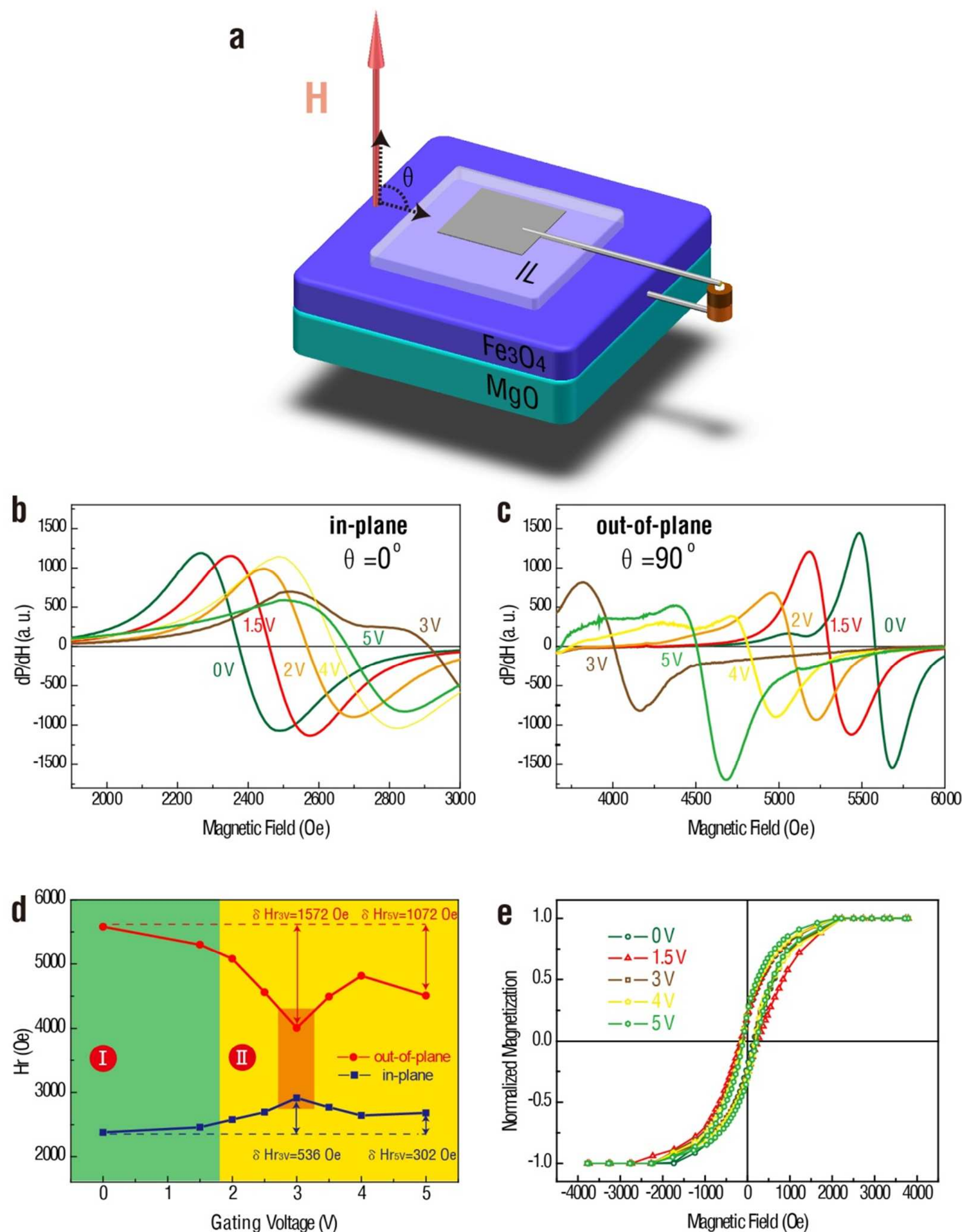

Figure 2. (a) The schematic of ESR measurement, and when θ=0 and 90° represent in-plane and out-of-plane, respectively. The in-plane and out-of-plane FMR spectra of Fe_3O_4/MgO heterostructure gated by IL were shown in (b) and (c), respectively. (d) In-plane and out-of-plane H_r as a function of applied V_g in both Region I and Region II. (e) The out-of-plane of *in*-situ VSM test of the Au/[DEME]$^+$[TFSI]$^-$/Fe_3O_4/MgO heterostructure at different V_g.

Figure 2 summaries the IL gating effect on the magnetic properties under various V_g in both Region I and Region II, which were measured in the X-band FMR cavity under N_2 gas protection[3,40], as shown in the schematic of Figure 2a. Figure 2b and Figure 2c show the in-plane and out-of-plane FMR spectra of the Au/[DEME]$^+$[TFSI]$^-$/Fe_3O_4/MgO heterostructure under E-field bias in Region I and Region II. The distinct in-plane and out-of-plane H_r shifts (spin dynamics change) were obtained and both the FMR shifts reached the maximum at V_g=3 V, corresponding to the maximum charges distribution at the interface as verified in Figure 1d. Figure 2d demonstrates the H_r dependence (both in-plane and out-of-plane) on V_g, covering the Region I and Region II. When V_g=3 V, the out-of-plane H_r shift reached its maximum of 1572 Oe (from 5580 Oe to 4008 Oe), corresponding to a large ME coefficient of 524 Oe/V. Meanwhile, an in-plane H_r change of 536 Oe with a ME coefficient of 178 Oe/V was also obtained. Compared with tunability of 234 Oe/V at V_g=5 V, the ME coefficient at 3 V is much greater due to the larger IL capacitance and surface charges accumulation at the interface, as confirmed in capacitance test of Figure 1d. The tendency of the ratio of Fe^{3+} to Fe^{2+} is further confirmed in the following analysis by EELS and XPS in Figure 4. Figure 2e presents the out-of-plane magnetic hysteresis loops of the IL-gated Fe_3O_4 obtained by vibrating sample measurements (VSM), from which we can find that Fe_3O_4 are always ferromagnetic during the gating process at different gating voltage. And the VSM curves without normalized saturation magnetization are shown in Supporting Information in Figure S2. The coercive field (H_c) almost keeps constant for all the V_g values applied. The

angular dependences of H_r at V_g=0 V and 1.5 V are also shown in Figure S3 (Supporting Information). It can be seen that, the H_r increased for angle<60° while it decreased for angle>60°.

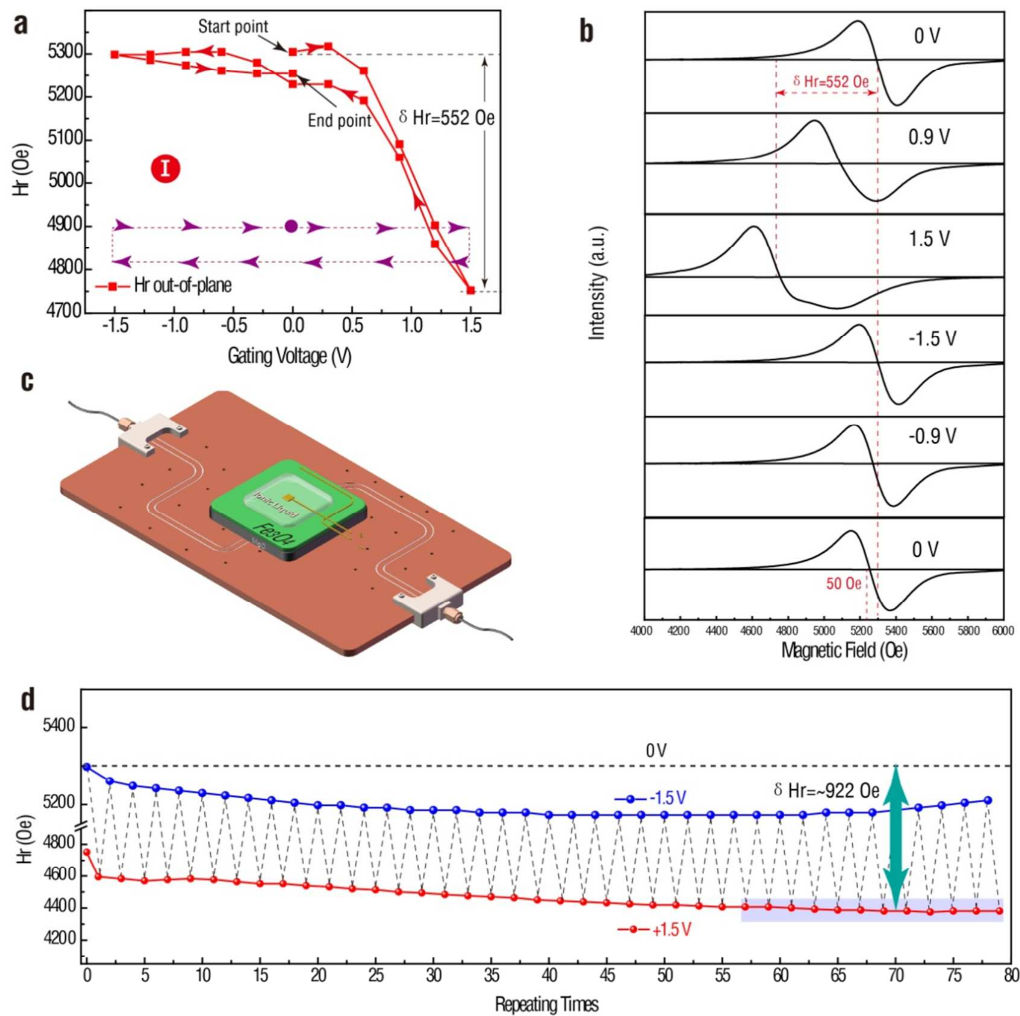

Figure 3. The reversibility test for the Au/[DEME]$^+$[TFSI]$^-$/Fe_3O_4/MgO heterostructure with V_g in Region I. (a) Out-of-plane H_r loop as a function of the V_g (gating voltage was changed from 0 V to +1.5 V, to -1.5 V, and back to 0 V, as shown by the violet dash loop). (b) The typical FMR curves of the Au/[DEME]$^+$[TFSI]$^-$/Fe_3O_4/MgO heterostructure along the out of plane direction for

one cycle as shown in (a) and the dash lines indicate the difference of 0 V and +1.5 V (c) The model diagram of Fe_3O_4 based voltage tunable spintronic devices. (d) Out-of-plane H_r shift of the Au/[DEME]$^+$[TFSI]$^-$/Fe_3O_4/MgO heterostructure as a function of V_g= ±1.5 V for 80 cycles.

The reversibility of the E-field tuning is a vital performance for realizing ME devices. In Figure 3, to verify the stability of the IL gating controlling of magnetism, the out-of-plane H_r shift of the Au/[DEME]$^+$[TFSI]$^-$/Fe_3O_4/MgO heterostructure as a function of ±1.5 V was tested for cycles. Firstly, the single cycle loop of the out-of-plane H_r as a function of gating voltage in Region I is displayed in Figure 3a, following the V_g sequence (from 0 V to +1.5 V, to -1.5 V and then back to 0 V at last, as shown by the violet dash loop). Only a positive V_g induced a large H_r shift. In contrast, under a negative V_g, the chemical valence could hardly change and affect the surface magnetism. The imbalanced VCMA change was also confirmed in our previous work on IL gating of metallic Co thin film[3]. The contour map of the out-of-plane FMR results at different V_g is illustrated in Figure S4a (Supporting Information), where the FMR intensity was plotted as a function of voltage (y axis) and applied magnetic field (x axis). Figure 3b shows the typical FMR curves in Figure 3(a) at different gating voltages. The maximum of tunability of 552 Oe is obtained at +1.5 V and 50 Oe difference is detected for one cycle gating voltage since the reversibility of the induced double layer electron cannot be perfect because ionic gating process always involves the limited electrochemical reaction and the charge

distribution after the gating voltage is applied/withdrawn is time-dependent. When negative gating voltage was applied, no electron injection or oxygen vacancy were produced due to the inverse EDL distribution at the surface, hence the ration of Fe^{2+} and Fe^{3+} keep constant as the initial state and almost no tunability was observed. Since the great coefficient of 368 Oe/V at low gating voltage, a realizable Fe_3O_4-based low-energy consumption spintronic prototype device is being designed based on the great tunability obtained in our research as shown in Figure 3c. Figure 3d shows voltage-induced out-of-plane H_r shift for 80 times test gated between +1.5 V and -1.5 V. Specifically, the stable H_r tuning of the +1.5 V IL gating occurred after dozens of cycles with reversible H_r shift as high as 922 Oe, corresponding to a greater VCMA coefficient of 615 Oe V^{-1}. The contour map of the out-of-plane FMR spectra for 80 cycles was shown in Figure S4b (Supporting Information). In short, the stable and maximum VCMA occurs after dozens of cycling tests, and the reason of the VCMA enhancement may be due to the stable charges distribution at the interface and almost unchanged roughness at the interface after dozens of cycles with applied V_g. The FMR spectra of in plane and out of plane with different cycles shown in Figure S4c-f (Supporting Information) indicated that even almost hundred of cycles the Fe_3O_4 films were also ferromagnetic as the initial state, which exhibited good reversibility. The 80-cycle reversibility test demonstrates great reversibility and shows the possibility to design the prototype to tunable spintronic devices.

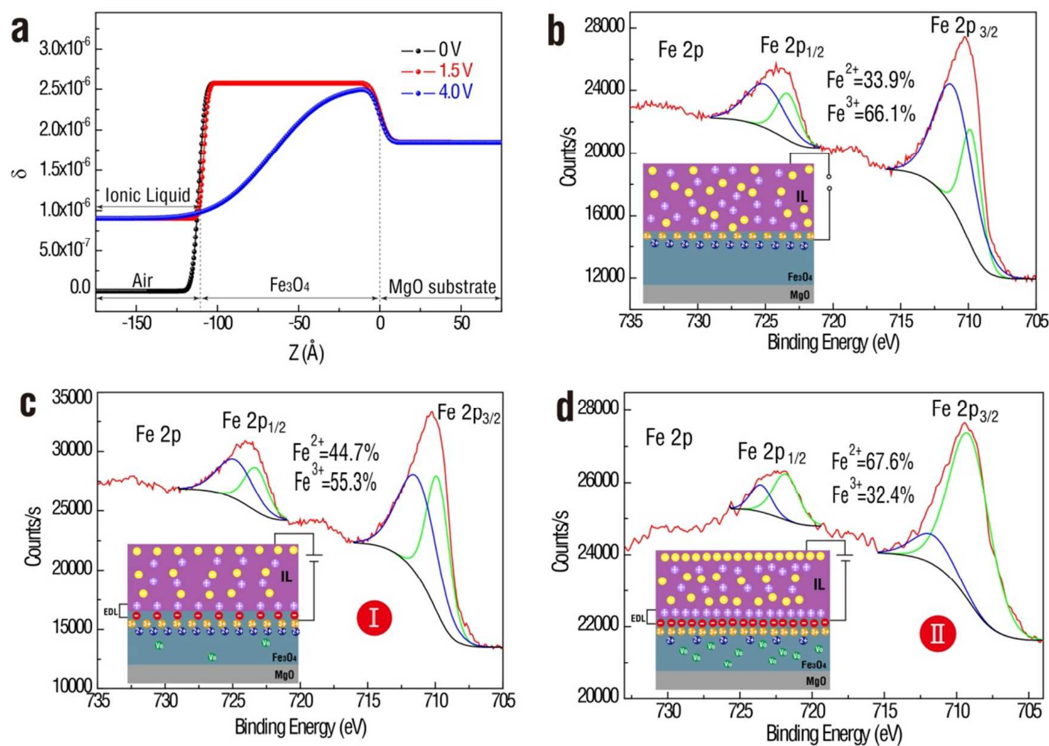

Figure 4. (a) Depth variation of dispersion part of refractive index (δ) of the measured XRR profile (plot line) at different gating voltage. (b-d) XPS spectra of Fe 2p for the ungated, +1.5 V and 4 V-gated samples. The insets in (b), (c) and (d) show the schematics of the Au/[DEME]$^+$[TFSI]$^-$/Fe_3O_4/MgO heterostructure in ungated state, gated Region I and Region II, respectively. Only Fe^{3+} at the interface was marked to simplify the changes in Fe^{3+} at the interface during the gating process in initial state, Region I and Region II in the insets of b-d.

To illustrate the changes of thickness and roughness of the Fe_3O_4 films, *in*-situ X-ray reflectivity (XRR) measurements were performed during the gating process. The Figure 4a shows the depth variation of dispersion part of refractive index (δ) obtained after fitting of the measured XRR profile which was shown in Supporting Information in Figure S5. As can be seen clearly that the thickness of the ungated

sample (111 Å) and 1.5 V gated sample (109 Å) has the almost identical thickness, which is mainly attributed to the change of the roughness when gating voltage was applied. The roughness decreased from 3.1 Å to 2.2 Å when gating voltage was increased from 0 V to 1.5 V. As for the 4.0V gated sample, drastic thickness decrease (66 Å) was observed due to the severe chemical reaction in Region II and the roughness also greatly increased. This may partly illustrate the outstanding reversibility performance up to 80 cycles although chemical reaction cannot be diametrically excluded in Region I. The structural analysis and interfacial valence states revealed by X-ray photoelectron spectroscopy (XPS) and electron energy loss spectroscopy (EELS) which are also displayed in Figure 4b-d and Supporting Information Figure S6. Since the state of IL-gated Fe_3O_4 sample will be kept long enough after the applied voltage was removed, we used samples which were applied gating voltage and then the ionic liquid was cleared at once for the structural and interfacial valence states analysis. Detailed EELS analysis and data are presented in Figure S6 (Supporting Information). The XPS experiments were performed for all the samples to reveal the interfacial valence change of the Fe ions. As shown in Figure 4b, the ungated sample has a Fe^{2+}/Fe^{3+} ratio of about 1:2, corresponding to the stoichiometry of the Fe_3O_4 thin film. The schematic in the inset of Figure 4(b) present the ungated state of the heterostructure. Under an E-field of +1.5 V, the percentage of Fe^{2+} ions increased from 33.9% to 44.7%, while that of Fe^{3+} decreased from 66.1% to 55.3%, as shown in Figure 4c, which may be attributed to the strong charge doping by under the high electric field induced by the interfacial electric double layer. As shown

in the inset of Figure 4c, EDL is formed at the interface due to the applied gating voltage. The generous doped electron at the interface may change the local electronic structure of Fe_3O_4, leading part of Fe^{3+} got electron and turned to Fe^{2+}, which results in a large VCMA through this interfacial ME effect. The observed reversible H_r tuning could be attributed to the reversible redox process of Fe^{3+} and Fe^{2+} originated from the electron doping and withdrawn when positive and negative V_g are applied alternately. Although we cannot absolutely exclude the electrochemical process in the Region I, it must be in a negligible scale according to the XRR results in Figure 4(a). The variation of Fe^{2+} and Fe^{3+} ions extracted from the XPS data coincides perfectly with the EELS data. However, when V_g=4 V was applied, outside of the electrochemical window, the IL reacted with Fe_3O_4 films and corroded the interface irreversibly, which reduced the Fe_3O_4 thickness greatly. The percentage of the Fe^{2+} ions for 4 V-gated samples was further increased to 67.6% while that of the Fe^{3+} ions decreased to 32.4% due to more doped electrons and electrochemical reaction, as shown in Figure 4d. Although a larger H_r shift was obtained, the processes were irreversible because of the irreversibility of the electrochemical processes. Meanwhile more oxygen vacancies will be greatly induced in this process as shown in the inset of Figure 4(d), which could also be proven by the XPS spectra of O 1s of the heterostructures gated at 0 V, 1.5 V and 4 V shown in Supporting Information in Figure S7. The surface morphology of the samples gated at different voltage was given in Figure S8 (Supporting Information), showing a negligible surface roughness change in Region I and a drastic increase of roughness in Region II.

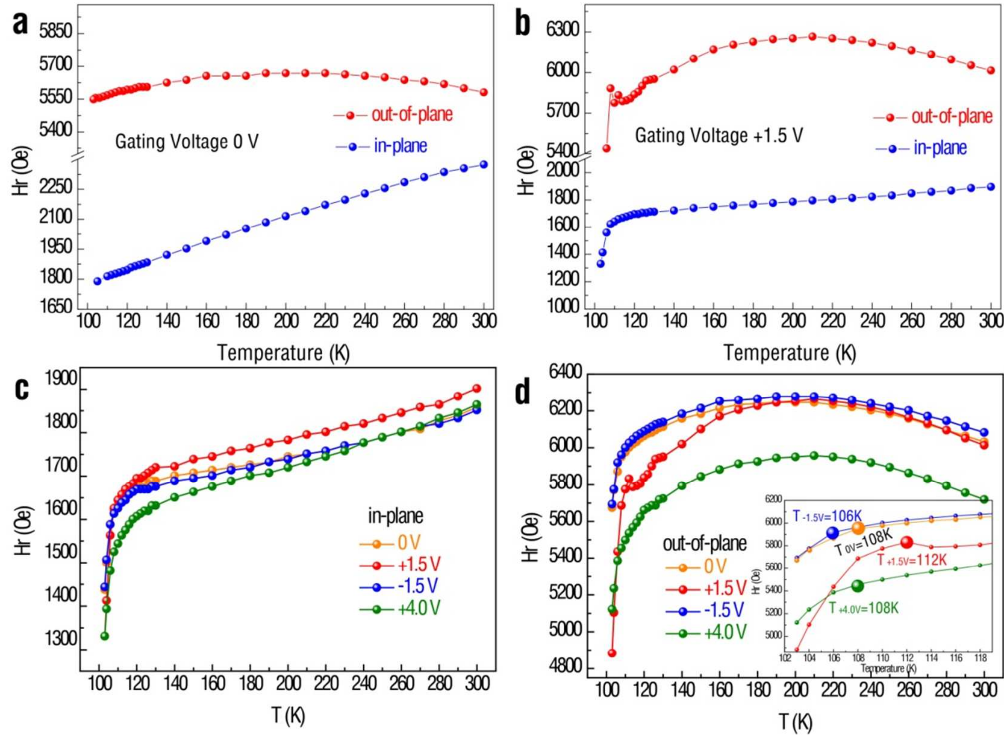

Figure 5. (a-b) Temperature-dependent H_r of the ungated (a) and gated with +1.5 V (b) Fe_3O_4 samples ~8 nm thick along both in-plane and out-of-plane directions. (c-d) Temperature dependent H_r of ungated and gated with different V_g Fe_3O_4 ~20 nm samples along the in-plane (c) and out-of-plane (d) directions. The inset in (d) shows the details at low temperature from 100 K to 118 K.

As a widely used conducting spin-polarized ferrimagnet, the characteristic Verwey metal-insulator transition of magnetite remains an active area of research[41-43]. The mechanism behind the Verwey transition is under a long-standing debate between charge ordering ('Wigner crystal') of the Fe^{2+}/Fe^{3+} cations on the octahedral sites and structural/orbital ordering. Here, the IL gating process as an external charge doping method provides a new approach to study the Verwey transition. Figure 5 shows temperature-dependent H_r of Fe_3O_4 with different thickness along in-plane and

out-of-plane direction under various V_g. The FMR measurements determined the Verwey transition temperature (V_T) precisely from the values of H_r. In Figure 5a, the Fe_3O_4 (~8 nm)/MgO heterostructure was tested in the temperature range from 300 K to 100 K and no V_T could be detected, which may be attributed to nano-size effect that smeared out the Verwey transition. It was reported that the Verwey transition disappears in Fe_3O_4 nanocrystals smaller than 6nm[44] due to the broken symmetry of the crystal structure and the presence of low-coordinated atoms at the surface. The different nanocrystal size in 8 nm films and 20 nm films may be the reason for the size-dependent Verwey transition in Figure 5a-b. Interestingly, with an applied V_g of +1.5 V, a distinct Verwey transition appeared as evidence by a sharp drop of H_r vs. T, for both the in-plane and out-of-plane configurations as shown in Figure 5b, demonstrating a voltage controllable Verwey transition. The in-plane and out-of-plane V_T was calculated from the FMR results as 108 K. Based on the EELS and XPS analyses in Figure 4, the ratio of Fe^{2+}/Fe^{3+} cations at the interface of gated sample has been changed compared with that of ungated samples. Charge doping from IL gating leads to the redistribution of the localized electrons over linear three-Fe-site units and induces large electrical polarization coupled to the magnetization, resulting in an E-field induced Verwey transition. Our experiments thereby offer another evidence in favor of the charge ordering (‘Wigner crystal’)-dominated phase transition theory[45,46] instead of the structural/orbit coupling which cannot be changed during IL gating process apparently. In Figure 5c-d, the quantitative E-field induced V_T was further investigated along the in-plane and out-of-plane directions for a thicker (~20 nm)

Fe_3O_4 film. A clear Verwey phase transition was detected from the in-plane temperature dependent H_r as shown in Figure 5c. Considering the smaller in-plane VCMA, the in-plane V_T changes indistinctly. Along the out-of-plane direction, however, the temperature-dependent H_r patterns are very different under various V_g, as represented in Figure 5d. These V_T values were estimated by finding the inflection points of the H_r - T curves (the inset of Figure 5d) as: 108 K (ungated), 106 K (-1.5 V-gated), 112 K (+1.5 V-gated) and 108 K (4 V-gated). The 6 K reversible voltage-induced out-of-plane V_T shift was observed, which is unneglectable within the IL chemical window. Under V_g=4 V outside the electrochemical window, V_T shifts back to 108 K, however, this result is not meaningful because of the film damage and . The related weak voltage-induced Verwey transition change of Fe_3O_4 film may due to that the IL gating process only affects the interface layer. We may conclude that the Verwey transition is indeed originated from charge ordering and the proportion of the Fe^{2+}/Fe^{3+} ions does influence the transition behavior just as other research reported[47]. As thus, IL gating method is not only an effective tool of VCMA, but also the method of modulation spin ordering such as the Verwey transition in magnetite thin films.

Conclusions

In summary, the VCMA of Au/$[DEME]^+[TFSI]^-/Fe_3O_4$/MgO heterostructure via IL gating is studied. Our results show that the magnetic properties of Fe_3O_4 thin film can be effectively controlled by IL gating, achieving a giant ME coupling tunability of 552 Oe corresponding to a high ME coefficient of 368 Oe/V with good reversible

performances. The reversible VCMA is induced by the ionic transition between Fe^{2+} and Fe^{3+} through IL charge doping, confirmed by the EELS and XPS analyses. The thickness changes of the films during the IL gating process indicate almost no chemical corrosion in Region I and give rise to excellent reversibility. Moreover, the Verwey transition temperature can be also shifted by up to 6 K by E-field, proving the viability of IL gating in the modulation of intrinsic spin ordering. This study provide a new way for designing smart spintronics devices with high effective low voltage manipulated VCMA and reversibility.

Conflicts of interest

There are no conflicts of interest to declare.

Acknowledgments

L. Zhang, W. X. Hou and G. H. Dong contributed equally to this work. The work was supported by the Natural Science Foundation of China (Grant No. 51472199, 11534015, and 51602244), the National 111 Project of China (B14040), the 973 Program (Grant No. 2015CB057402), the Fundamental Research Funds for the Central Universities. The authors acknowledge the support from the International Joint Laboratory for Micro/Nano Manufacturing and Measurement Technologies. M. Liu and Z. Zhou were supported by the China Recruitment Program of Global Youth Experts. W. Chen was supported by the US Department of Energy, Office of Science, Materials Sciences and Engineering Division. Z.-G. Ye acknowledges the support

from the Natural Sciences at Engineering Research Council of Canada (NSERC, Grant No. 203773).

Experimental Section

Thin Film Growth Fe_3O_4 thin films were deposited onto 5 mm × 5 mm × 0.5 mm MgO (001) substrates by pulsed laser deposition (PLD) using a home-made α-Fe_2O_3 ceramic target. The homogeneous and dense ceramic target with a diameter of 30 mm and a thickness of 5 mm was calcined and sintered by conventional solid-state reaction at 1050 ^oC for 2h. Krypton fluoride (KrF) excimer laser (Lambda Physik COMPEX PRO 205 F) with a 248 nm wavelength was employed and focused onto the ceramic target and operated with a laser energy density of 240 mJ per pulse laser beam energy at a repetition rate of 5 Hz at 9 $\times 10^{-4}$ Pa without the insertion of oxygen at 450 ^oC. The growth process took 10~50 minutes to deposit Fe_3O_4 with different thicknesses. No further *in*-situ annealing was carried out.

Phase and Structure Characterization: High-resolution X-ray diffraction (PANalytical, X'Pert MRD) and Raman scattering were performed to determine the crystal structure of the Fe_3O_4 thin films. The surface analysis of the Fe_3O_4 films before and after gating were conducted by X-ray photoelectron spectroscopy (XPS) with 150-180 W Al anode and a 100 meV step. The film morphologies before and after gating with different voltages were characterized via atomic force microscope (AFM, Bruker, Dimension Icon). The interface structure of the as-grown Fe_3O_4 films, gated at 1.5 V and gated at 4 V, were imaged by spherical aberration correction

transmission electron microscope (JEM-ARM200F, JEOL).

Device Fabrication: The ionic liquid N,N-diethyl-N-(2-methoxyethyl)-N-methylammonium bis-(trifluoromethylsulphonyl)-imide (DEME-TFSI, Kanto Chemical Co.) was dropped onto the Fe_3O_4 films and then confined into a 3 mm × 3 mm × 1 mm chemically inert cell. The gating voltage was applied to the system by two gold wires (0.1 mm in diameter), one was contacted with Fe_3O_4 magnetic films and the other was contacted with IL through the chemically inert cell. The cell was put into the FMR chamber and the test process was conducted under N_2 as protecting gas.

Magnetic Measurement: *In*-situ voltage-controlled magnetic anisotropy measurements were carried out by electron paramagnetic resonance (EPR, JES-FA200, JEOL RESONANCE Inc.) and vibrating sample magnetometer (VSM), where the angle between the film plane and the external magnetic field was precisely determined. The gating voltage was applied by an Agilent 2901A Electrometer. These tests were conducted after 5 minutes when the gating voltage was applied to the system in order to balance the movements caused by thermal diffusion or E-field driven.

Electrical and Capacitance Measurements: The electrochemical window test was performed in a cavity filled with nitrogen gas, with the assistance of a B2901A Precision Source/Measure Unit at 4 mV s^{-1}. The capacitance measurements were carried out using an Agilent E4980A Precision LCR Meter at room temperature from 20 Hz to 1 kHz with amplitude of 100 mV. The DC bias was set according to the gating voltage of the magnetic measurement. During the measurement, the system

was also located in the FMR chamber in order to maintain the same atmosphere. The IL was located in a 3 mm × 3 mm × 1 mm chemically inert cell, therefore, the capacitance was calculated using a 9 mm^2 surface area.

References

[1] J.-M. Hu, L.-Q. Chen, C.-W. Nan, *Adv. Mater.*, 2016, **28**, 15-39.

[2] A. Molinari, H. Hahn, R. Kruk, *Adv. Mater.*, 2018, **30**, 1703908.

[3] S. Zhao, Z. Zhou, B. Peng, M. Zhu, M. Feng, Q. Yang, Y. Yan, W. Ren, Z.-G. Ye, Y. Liu, M. Liu, *Adv. Mater.*, 2017, **29**, 1606478.

[4] D. Chiba, S. Fukami, K. Shimamura, N. Ishiwata, K. Kobayashi, T. Ono, *Nat. Mater.*, 2011, **10**, 853-856.

[5] M. Wang, W. Cai, K. Cao, J. Zhou, J. Wrona, S. Peng, H. Yang, J. Wei, W. Kang, Y. Zhang, J. Langer, B. Ocker, A. Fert, W. Zhao, *Nat. Commun.*, 2018, **9**, 671.

[6] Q. Yang, L. Wang, Z. Zhou, L. Wang, Y. Zhang, S. Zhao, G. Dong, Y. Chen, T, Min, Z. Hu, W. Chen, K. Xia, M. Liu, *Nat. Commun.*, 2018, **9**, 991.

[7] .Q. Yang, Z. Zhou, L. Wang, H. Zhang, Y. Cheng, Z. Hu, B. Peng, and M. Liu, *Adv. Mater.*, 2018, **30**, 1800449.

[8] S. Zhao, L. Wang, Z. Zhou, C. Li, G. Dong, L. Zhang, B. Peng, T. Min, Z. Hu, J. Ma, W. Ren, Z.-G. Ye, W. Chen, P. Yu, C.-W. Nan, M. Liu, *Adv. Mater.*, 2018, **30**, 1801639.

[9] L. Yin, X. Wang, W. Mi, *ACS Appl. Mater. Interfaces*, 2017, **9**, 15887-15892.

[10] L. Yin, X. Wang, W. Mi, *Appl. Phys. Lett.*, 2017, **111**, 032404.

[11] M. Liu, O. Obi, J. Lou, Y. Chen, Z. Cai, S. Stoute, M. Espanol, M. Lew, X. Situ, K. S. Ziemer, V. G. Harris, N. X. Sun, *Adv. Funct. Mater.*, 2009, **19**, 1826-1831.

[12] J. Lou, M. Liu, D. Reed, Y. Ren, N. X. Sun, *Adv. Mater.*, 2009, **21**, 4711-4715.

[13] S. Li, G.-X. Miao, D. Cao, Q. Li, J. Xu, Z, Wen, Y. Dai, S. Yan, Y. Lü, *ACS Appl. Mater. Interfaces*, 2018, **10**, 8853-8859.

[14] W. Li, H. Yan, X. J. Chai, S. H. Wang, X. L. Dong, L. X. Ren, C. L. Chen, K. X. Jin, *Appl. Phys. Lett.*, 2017, **110**, 192411.

[15] R. O. Cherifi, V. Ivanovskaya, L. C. Phillips, A. Zobelli, I. C. Infante, E. Jacquet, V. Garcia, S. Fusil, P. R. Briddon, N. Guiblin, A. Mougin, A. A. Unal, F. Kronast, S. Valencia, B. Dkhil, A. Barthelemy, M. Bibes, *Nat. Mater.*, 2014, **13**, 345-351.

[16] J.-J. Wang, H.-B. Huang, T.J.M. Bayer, A. Moballegh, Y. Cao, A. Klein, E. C. Dickey, D. L. Irving, C. A. Randall, L.-Q. Chen, *Acta Mater.*, 2016, **108**, 229-240.

[17] U. Bauer, L. Yao, A. J. Tan, P. Agrawal, S. Emori, H. L. Tuller, S. van Dijken, G. S. D. Beach, *Nat. Mater.*, 2015, **14**, 174-181.

[18] C.-G. Duan, S. S. Jaswal, E. Y. Tsymbal, *Phys. Rev. Lett.*, 2006, **97**, 047201.

[19] T. Nan, Z. Zhou, M. Liu, X. Yang, Y. Gao, B. A. Assaf, H. Lin, S. Velu, X. Wang, H. Luo, J. Chen, S. Akhtar, E. Hu, R. Rajiv, K. Krishnan, S. Sreedhar, D. Heiman, B. M. Howe, G. J. Brown, N. X. Sun, *Sci. Rep.*, 2014, **4**, 3688.

[20] J. Walter, H. Wang, B. Luo, C. D. Frisbie, C. Leighton, *ACS Nano*, 2016, **10**, 7799-7810.

[21] W. Shi, J. Ye, J. G. Checkelsky, C. Terakura, Y. Iwasa, *Adv. Func.Mater.*, 2014, **24**, 2005-2012.

[22] T. Hirai, T. Koyama, A. Obinata, Y. Hibino, K. Miwa, S. Ono, M. Kohda, D. Chiba, *Appl. Phys. Express*, 2016, **9**, 063007.

[23] Y. J. Zhang, J. T. Ye, Y. Yornogida, T. Takenobu, Y. Iwasa, *Nano Lett.*, 2013, **13**, 3023-3028.

[24] T. Koide, H. Miyauchi, J. Okamoto, T. Shidara, A. Fujimori, H. Fukutani, K. Amemiya, H. Takeshita, S. Yuasa, T. Katayama, Y. Suzuki, *Phys. Rev. Lett.*, 2001, **87**, 257201.

[25] H. Y. Hwang, Y. Iwasa, M. Kawasaki, B. Keimer, N. Nagaosa, Y. Tokura, *Nat. Mater.*, 2012, **11**, 103-113.

[26] Y. Yamada, K. Ueno, T. Fukumura, H. T. Yuan, H. Shimotani, Y. Iwasa, L. Gu, S. Tsukimoto, Y. Ikuhara, M. Kawasaki, *Science*, 2011, **332**, 1065-1067.

[27] B. Cui, C. Song, G. A. Gehring, F. Li, G. Wang, C. Chen, J. Peng, H. Mao, F. Zeng, F. Pan, *Adv. Funct. Mater.*, 2015, **25**, 864-870.

[28] M. Weisheit, S. Faehler, A. Marty, Y. Souche, C. Poinsignon, D. Givord, *Science*, 2007, **315**, 349-351.

[29] T. Maruyama, Y. Shiota, T. Nozaki, K. Ohta, N. Toda, M. Mizuguchi, A. A. Tulapurkar, T. Shinjo, M. Shiraishi, S. Mizukami, Y. Ando, Y. Suzuki, *Nat. Nanotech.*, 2009, **4**, 158-161.

[30] Y. Saito, Y. Iwasa, *ACS Nano*, 2015, **9**, 3192-3198.

[31] M. N. Grisolia, J. Varignon, G. Sanchez-Santolino, A. Arora, S. Valencia, M. Varela, R. Abrudan, E. Weschke, E. Schierle, J. E. Rault, J. P. Rueff, A. Barthelemy, J. Santamaria, M. Bibes, *Nat. Phys.*, 2016, **12**, 484-493.

[32] C. Bi, Y. Liu, T. Newhouse-Illige, M. Xu, M. Rosales, J. W. Freeland, O. Mryasov,

S. Zhang, S. G. E. te Velthuis, W. G. Wang, *Phys. Rev. Lett.*, 2014, **113**, 267202.

[33] N. Lu, P. Zhang, Q. Zhang, R. Qiao, Q. He, H.-B. Li, Y. Wang, J. Guo, D. Zhang, Z. Duan, Z. Li, M. Wang, S. Yang, M. Yan, E. Arenholz, S. Zhou, W. Yang, L. Gu, C.-W. Nan, J. Wu, Y. Tokura, P. Yu, *Nature*, 2017, **546**, 124-128.

[34] M.-T. Chang, L.-J. Chou, C.-H. Hsieh, Y.-L. Chueh, Z. L. Wang, Y. Murakami, D. Shindo, *Adv. Mater.*, 2007, **19**, 2290-2294.

[35] E. Lima, A. L. Brandl, A. D. Arelaro, G. F. Goya, *J. Appl. Phys.*, 2006, **99**, 083908.

[36] X.-L. Wu, T. Wen, H.-L. Guo, S. Yang, X. Wang, A.-W. Xu, *ACS Nano*, 2013, **7**, 3589-3597.

[37] S. Schmaus, A. Bagrets, Y. Nahas, T. K. Yamada, A. Bork, M. Bowen, E. Beaurepaire, F. Evers, W. Wulfhekel, *Nat.Nanotech.*, 2011, **6**, 185-189.

[38] R. Bliem, E. McDermott, P. Ferstl, M. Setvin, O. Gamba, J. Pavelec, M. A. Schneider, M. Schmid, U. Diebold, P. Blaha, L. Hammer, G. S. Parkinson, *Science*, 2014, **346**, 1215-1218.

[39] C. Corot, P. Robert, J.-M. Idee, M. Port, *Adv. Drug Deliver. Rev.*, 2006, **58**, 1471-1504.

[40] H. Yuan, H. Shimotani, A. Tsukazaki, A. Ohtomo, M. Kawasaki, Y. Iwasa, *J. Am. Chem. Soc.*, 2010, **132**, 6672-6678.

[41] E. J. W. Verwey, *Nature*, 1939, **144**, 327-328.

[42] E. J. Verwey, P. W. Haayman, F. C. Romeijn, *J. Chem. Phys.*, 1947, **15**, 181-187.

[43] M. S. Senn, J. P. Wright, J. P. Attfield, *Nature*, 2012, **481**, 173-176.

[44] J. Lee, S. G. Kwon, J.-G. Park, T. Hyeon, *Nano Lett.*, 2015, **15**, 4337-4342.

[45] H. T. Jeng, G. Y. Guo, D. J. Huang, *Phys Rev. Lett.*, 2004, **93**, 156403.

[46] J. P. Wright, J. P. Attfield, P. G. Radaelli, *Phys. Rev. B*, 2002, **66**, 214422.

[47] J. J. I. Wong, A. G. Swartz, R. Zheng, W. Han, R. K. Kawakami, *Phys. Rev. B*, 2012, **86**, 060409.

In this manuscript, we demonstrate a new concept of low voltage (1.5 V) modulation of spin dynamics in ionic liquid-gated Au/$[DEME]^+[TFSI]^-$/Fe_3O_4/MgO heterostructure. This low voltage gating method has an excellent reversibility. The existing concept of modulating the spin dynamics is strain-mediated, which requires hundreds of driving voltage. In comparison, the ionic liquid modulation method reduces the gating voltage in a significant manner. Here, a precisely-determined 552 Oe spin dynamics modulation, corresponding to a large magnetoelectric (ME) tunability of 368 Oe/V with good reversibility up to 80 cycles was obtained, which is 2 orders of magnitude greater than that of strain-mediated ME structures in previous reports. The large ME tunability comes from a relative new mechanism - the voltage induced valence state switching of Fe ions in Fe_3O_4. This work throws light on the understanding of spin dynamics modulation in magnetic oxides and paves a way toward high performance, low voltage tunable spintronic applications.

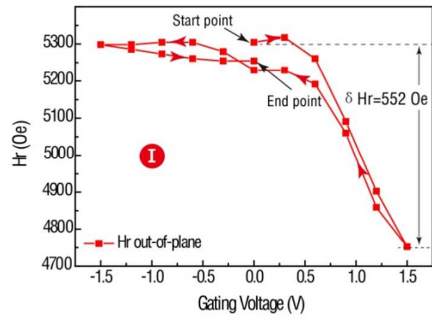

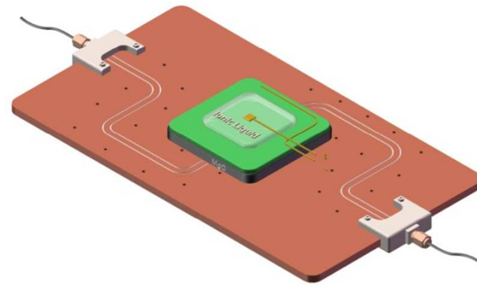

A giant ME coupling tunability of 552 Oe at 1.5 V corresponding to a high ME coefficient of 368 Oe/V with a good reversibility can be effectively controlled by IL gating in Fe_3O_4 thin film. These findings make it a possibility to design the prototype to tunable spintronic/microwave devices